Five-Fingered Haptic Interface Robot: HIRO III

Takahiro Endo, *Member*, *IEEE*, Haruhisa Kawasaki, *Senior Member*, *IEEE*, Tetsuya Mouri, *Member*, *IEEE*, Yasuhiko Ishigure, Hisayuki Shimomura, Masato Matsumura, and Kazumi Koketsu

Abstract—This paper presents the design and characteristics of a five-fingered haptic interface robot named HIRO III. The aim of the development of HIRO III is to provide a high-precision three-directional force at the five human fingertips. HIRO III consists of a 15-degrees-of-freedom (DOF) haptic hand, a 6-DOF interface arm, and a control system. The haptic interface, which consists of a robot arm and hand, can be used in a large workspace and can provide multipoint contact between the user and a virtual environment. However, the following problems peculiar to a multi-DOF robot have arisen: a large amount of friction, a backlash, and the presence of many wires for many motors and sensors. To solve these problems, a new mechanism and a wire-saving control system have been designed and developed. Furthermore, several experiments have been carried out to investigate the performance of HIRO III. These results show the high-precision force display and great potential of HIRO III.

Index Terms—Design, haptic I/O, interfaces, virtual reality.

1 Introduction

Multifingered haptic interfaces that allow multipoint contact between users and a virtual environment have greater potential for various applications than do single-point haptic interfaces. The multipoint interaction allows a user to perform natural actions, such as grasping, manipulation, and exploration of virtual objects, and such interaction will dramatically increase the believability of the haptic experience [1], [2], [3]. In performing activities in our daily lives, we usually use multiple fingers and grasp and manipulate objects with dexterity. Furthermore, the exploration of an object is affected by the number of fingers used, and exploration with multiple fingers is more effective than exploration with a single finger [4], [5], [6]. Thus, it is important to be able to exert force at multiple fingertips in order to generate a sensation that is highly realistic to human beings. In addition, since we are familiar with activities that involve multiple fingers, the multifingered haptic interface can be used naturally and without extensive familiarization. Based on these considerations, the development of a multifingered haptic interface has been eagerly anticipated and is expected to further haptics in virtual environments.

- *T. Endo, H. Kawasaki, and T. Mouri are with the Department of Human and Information Systems, Gifu University, Gifu, 501-1193 Japan. E-mail: {tendo, h_kawasa, mouri}@gifu-u.ac.jp.*
- *Y. Ishigure is with the Marutomi Seiko Co., Ltd., Aza-Ikuda, Kurachi, Seki-shi, Gifu, 501-3936, Japan. E-mail: ishigure@maru-tomi.co.jp.*
- *H. Shimomura is with the Dainichi Co., Ltd., Kani-City, Gifu, 509-0249 Japan. E-mail: ana@kk-dainichi.co.jp.*
- *M. Matsumura is with the e-Valley Co., Ltd., Showaku, Nagoya, 466-0059 Japan. E-mail: matsumura@e-valley.co.jp.*
- *K. Koketsu is with the Tec Gihan Co., Ltd., Nishinohata, Okubo-cho, Uji-city, Kyoto 611-0033, Japan. E-mail: k.koketsu@tecgihan.co.jp.*

Manuscript received 13 Feb. 2010; revised 27 May 2010; accepted 4 June. 2010; published online 9 Dec. 2010.
Recommended for acceptance by A. Frisoli.
For information on obtaining reprints of this article, please send e-mail to: toh@computer.org, and reference IEEECS Log Number TH-2010-02-0006.
Digital Object Identifier no. 10.1109/ToH.2010.62.

Although the development of a multifingered haptic interface continues to pose design and technical challenges [7], [8], several multifingered haptic interfaces have been pursued aggressively [2], [3], [5], [7], [9], [10], [11], [12], [13], [14], [15], [16], [17], [18], [19], [20], [21], [22], [23], [24], [25] because of their potential effectiveness and usefulness. The current multifingered haptic interfaces can be divided into two groups: grounded-type haptic interfaces [2], [3], [5], [9], [10], [11], [12], [13], [14], [15], [16], [17], [18], [19], [20], [21], and ungrounded-type (exoskeleton-type) haptic interfaces [7], [22], [23], [24], [25]. The exoskeleton-type haptic interface has a large workspace, but with this interface it is difficult to present three-directional forces or the weight of virtual objects through the fingertips because the hand mechanism is mounted on the back of a human hand, and the exerted force is only a one-directional force. For example, when the haptic interface generates force by using a wire, the force applied to the operator is only exerted in the direction that the wire pulls. Thus, it is difficult to present a delicate force or the weight of virtual objects. As exceptions, A. Frisoli et al. [7] and T. Koyama et al. [25] have developed exoskeleton-type haptic interfaces that can present three-directional force at human fingertips. They used a serial link mechanism in the design of the haptic interface and were able to present a three-directional force at two or three of the user's fingertips. However, the mechanism is mounted on the user's hand, and thus it is difficult to present the weight of virtual objects, and it is difficult to use the haptic interface for a long time because of its weight [3], [26].

In contrast, the grounded-type haptic interface generally has a fairly small workspace compared with the ungrounded-type haptic interface. However, a grounded-type haptic interface consisting of an arm and fingertips can be used in a large workspace [2], [3], [16], [17], [18], [19], [20], [21]. Barbagli et al. [2] and Najdovski et al. [3] have developed a multifingered haptic interface that consists of an arm and a gripper at the end of the arm. Unlike the haptic interface, which achieves multipoint interaction by

combining two or three haptic devices in parallel [13], [14], [15], the haptic interface [2], [3] can be used throughout a large workspace. However, the gripper is specialized for the purpose of grasping. So the interface allows the user to grasp a virtual object via a simple open-close movement, but the operator cannot grasp/manipulate an arbitrarily shaped virtual object with dexterity. Furthermore, most of the above haptic interfaces consist of a hand-exoskeleton-and-arm [16], [17], [18] or a hand-and-arm-exoskeleton [19], [20] system, and thus, the interfaces have the same problems as the exoskeleton type haptic interface. As a minority case, Yokokohji et al. [21] proposed the concept of an encountered-type haptic interface for human grasping. Although this device would be an ideal haptic interface, it has proven to be difficult to achieve using the present technology.

We concluded that the desirable attributes for a haptic interface include the following: The haptic interface must be safe, function in a wide space, and present not only three-directional force at the contact points but also the weights of virtual objects. In addition, it should neither cause an oppressive feeling when attached to the user's hand, nor should it represent its own weight. To meet these requirements, we have developed multifingered haptic interface robots that are placed opposite a human hand, known as HIRO [27] and HIRO II$^+$ [28]. Most haptic devices have a low reduction ratio, which permits impedance control without the use of a force sensor. However, this requires a large mechanism and entails difficulty in construction. Therefore, HIRO and HIRO II$^+$ have high reduction mechanisms and require a force sensor on each haptic fingertip. Although the haptic interface with a robot hand allows multipoint interaction, the robot hand is a multi-DOF device, which means that many motors, sensors, and amplifiers are needed. Because of the many wires required for the motors and sensors, it is difficult to miniaturize the control system and to operate the interface smoothly.

To provide high-precision force representation and to meet the functionality requirements, including light weight, low friction, low backlash, compactness, and so on [29], we consider the following attributes to be important: 1) a mechanical design that reduces friction and backlash, 2) a wire-saving control system, and 3) high-precision three-axis force sensors. With these concerns in mind, we have newly developed a five-fingered haptic interface robot, HIRO III. It consists of a haptic hand with five haptic fingertips, an interface arm, and a control system. To satisfy item 1), a new mechanism for the haptic hand and interface arm was designed that has accomplished the following: a reduction of the static friction, greater compactness, an improved layout of the joints, and a connection method for the touch between the human fingertips and the haptic fingertips. To reduce the number of wires and to increase the compactness of the haptic interface, we have newly developed a wire-saving control system, which consists of an interface FPGA circuit, a force sensor amplifier circuit, and a motor amplifier circuit. To present the force at the five human fingertips, HIRO III requires 21 motors, 21 encoders, and five force sensors. Because of this, the communication cables between HIRO III and its control PC include a total of 212 wires. However, our new wire-saving control system was installed in HIRO III. The force sensor, encoder, and motor signals are inputted into the wire-saving system and communicate to the control PC on an LAN. Therefore, we were able to reduce the number of wires from 212 to 20. Thus, item 2) has been satisfied. We previously developed the wire-saving control system and the high-precision three-axis force sensor, which correspond to item 3), for HIRO II$^+$ [30]. However, the interface FPGA circuit and the motor driver consist of several circuits, and thus are not compact. Furthermore, we were not able to obtain a high-precision force presentation at the five human fingertips in the experiments with HIRO II$^+$.

Fig. 1. Five-fingered haptic interface robot: HIRO III. A user connects his/her five fingertips to HIRO III through passive spherical permanent magnet joints.

In this paper, we describe the development of a five-fingered haptic interface robot, HIRO III, which was designed in accordance with the above three items, and our experimental investigation of its performance. This paper is organized as follows: In the next section, we introduce the mechanical design of HIRO III. Section 3 presents the newly developed control system for HIRO III. The experimental results described in Section 4 demonstrate the high potential of HIRO III. Finally, Section 5 presents our conclusions.

2 Mechanical Design of HIRO III

The five-fingered haptic interface robot, HIRO III, consisting of a five-fingered haptic hand and an interface arm, is shown in Fig. 1. HIRO III can present a three-directional force at five human fingertips. It is placed opposite a human hand, and the haptic fingertips are connected to the human fingertips through passive spherical magnet joints. This section presents the mechanical design of HIRO III.

2.1 Haptic Hand

The haptic hand is constructed of five haptic fingers and a handbase. The structure of the haptic hand is shown in Fig. 2, and its specifications are shown in Table 1. Each finger has three joints, allowing three DOF. The first joint relative to the handbase allows abduction/adduction, while the second and third joints allow flexion/extension. All joints are driven

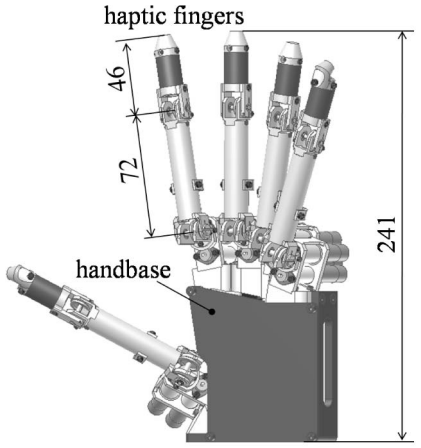

Fig. 2. Structure of haptic hand.

TABLE 1
Specifications of the Haptic Hand

Hand	Number of fingers		5
	Degrees of freedom		15 [DOF]
	Weight including wire-saving control system		under 0.78 [kg]
Fingers	Degrees of freedom		3 [DOF]
	Weight		under 0.12 [kg]
	Maximun output force		over 3.6 [N]
	Maximun velocity		over 0.2 [m/s]
	Workspace		Thumb:705, Other: 587 [cm^3]
	Operating angle	1st	Thumb:-36~36, Other:-30~30 [deg]
		2nd / 3rd	-35~90 / 0~112 [deg]

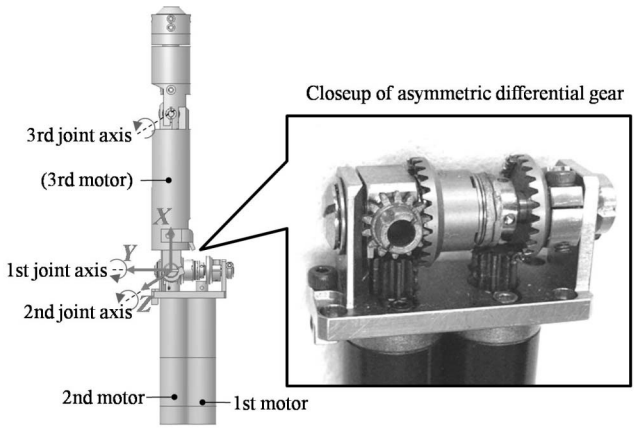

Fig. 3. Haptic finger of HIRO II$^+$.

by DC motors with gear and rotary encoders, where the gear consists of the gearhead of the motor and the gear of the transmission mechanism. Another important issue is the installation of force sensors. To read the finger loading forces, a previously developed three-axis force sensor [30] is installed in the second link of each finger.

2.1.1 Haptic Fingers

The haptic fingers of HIRO III are superior to those of HIRO II$^+$ in the following ways: 1) the static friction at the first and second joints of each finger has been reduced; and 2) the connecting position between the human fingertip and the haptic fingertip has been changed. The haptic finger of HIRO II$^+$, which is shown in Fig. 3, was designed based on an anthropomorphic robot hand [31]. As stated above, each

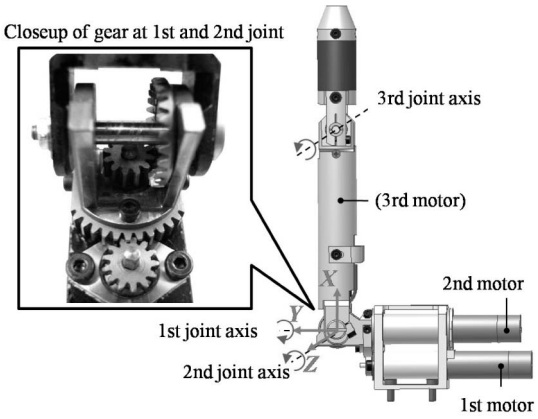

Fig. 4. Haptic finger of HIRO III.

TABLE 2
Specifications of the Haptic Finger Motors

Joint	Part number	Nominal torque [mNm]	Nominal current [A]	Gear ratio(*)
1st / 2nd / 3rd	maxon DC motor RE10 256105	1.54	0.176	768 / 554.7 / 140.8

(*) The gear consists of the gearhead of the motor and the gear of the transmission mechanism.

TABLE 3
Backlash and Friction Torque of the Haptic Finger

	Joint	HIRO II$^+$	HIRO III
Backlash [deg]	1st / 2nd / 3rd	0.49 / 1.07 / 0.72	0.47 / 0.94 / 0.75
Static friction torque [mNm]	1st / 2nd / 3rd	0.28 / 0.31 / 0.07	0.14 / 0.14 / 0.08

finger has three joints, allowing three DOF. To orthogonalize the first joint axis to the second joint axis, an asymmetric differential gear was adopted. This increased the compactness of the mechanism but provoked a large amount of friction and a backlash, and it required a great deal of maintenance. Even if the differential gear was useful for the robot hand, it had crucial disadvantages for the haptic interface. Therefore, we developed new haptic fingers in which each axis is independently driven without the differential gear. To realize an operation similar to that of HIRO II$^+$ without using the differential gear, we placed the motors on the shell side of the hand palm, as shown in Fig. 4. The specifications of the motors are listed in Table 2.

To investigate the effectiveness of the mechanism, we measured the backlash and the static friction at the joints. To investigate the backlash, we measured the free running angle of the joint. Note that all links were fixed with a jig. The free running angle of clockwise (CW) and counterclockwise (CCW) rotation was alternatively measured five times, and the average value was calculated. To assess the static friction torque, we measured the torque, where the joint began to move. The static friction torque of CW and CCW rotation was alternatively measured five times, and we obtained the average value. Table 3 shows the measurement results. In terms of the backlash, there was no large difference between the haptic fingers of HIRO II$^+$ and those of HIRO III. For the haptic fingers of HIRO III, we used the same motor and motor gearhead as in the haptic fingers of HIRO II$^+$, and thus the obtained backlash is the backlash of the motor gearhead, which would be difficult to improve by altering only the

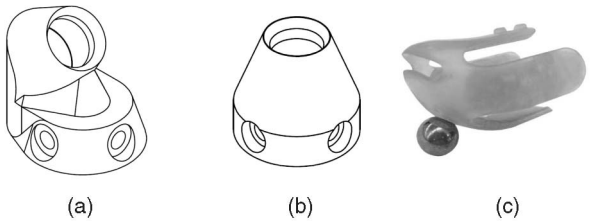

Fig. 5. Haptic fingertips. (a) Thumb and pinky. (b) Other fingers. (c) Finger holder.

transmission mechanism. On the other hand, the static friction of the first and second joints was reduced by 50 percent and 45 percent, respectively. In HIRO III, we eliminated the asymmetric differential gear and developed a new mechanism in which each axis is independently driven. This reduced the number of stages of the gear mechanism and reduced that weight of the joints. These features combine to reduce the friction at the first and second joints. Here, note that there is no change to the transmission mechanism at the third joint. Therefore, there is no large difference at the third joint.

We also improved the connecting position between the human and haptic fingertips. In particular, we changed the fingertip form of the thumb and pinky, as shown in Fig. 5. To manipulate the haptic interface, the user wears a finger holder (Fig. 5c) on each of his/her fingertips. The finger holder has a sphere which, when attached to the permanent magnet at the fingertip, forms a passive spherical joint. The role of the passive spherical joint attached to the permanent magnet is to adjust the differences between the orientations of the human and haptic fingers and to ensure that the operator can remove his/her fingers from the haptic interface if it malfunctions. The permanent magnet at the fingertip is in a hole, as shown in Figs. 5a and 5b. The entire

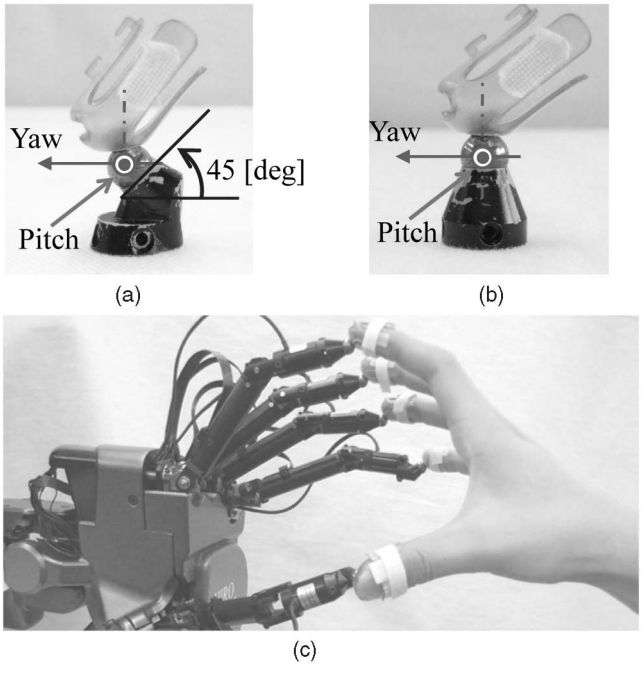

Fig. 6. Connection between finger holder and haptic fingertip. (a) Thumb and pinky. (b) Other fingers. (c) Close-up photo of the user's hand in the interface.

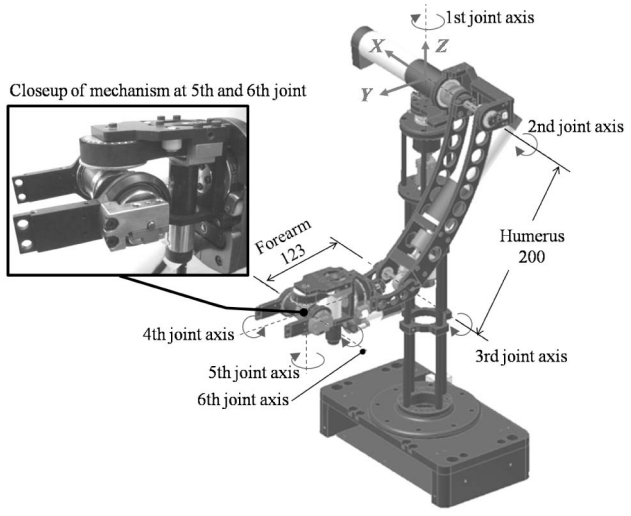

Fig. 7. Structure of the interface arm of HIRO III.

fingertip of HIRO II$^+$ is shown in Fig. 5b. However, when a user performs natural actions such as grasping, the thumb and pinky often move outside the workspace. By diagonally moving the contact point of the thumb and pinky, we solved this problem. In other words, we moved the contact point so that it is oriented 45 degree from horizontal (see Fig. 6). We then obtained a working space of the finger holder for the thumb and pinky fingertips with a pitch axis of -33 to 102 degrees and a yaw axis of -78 to 78 degrees. Here, the working space of the finger holder for the other fingertips has a pitch axis of -80 to 72 degrees and a yaw axis of -78 to 78 degrees. As a guide, we show a closeup photo of the connection between the user's hand and the interface in Fig. 6c.

2.1.2 Haptic Finger Layout

For the finger layout, we duplicated the method used in HIRO II$^+$, which optimized the design performance index (see [28] for details). In HIRO II$^+$, an asymmetric differential gear was adopted, and thus the first and second motors of the fingers other than the thumb were stored inside the handbase. For HIRO III, we used the same finger layout as in HIRO II$^+$ with the first and second motors being placed at the shell side of the handbase, as shown in Fig. 4. Therefore, we were able to create space inside the handbase, where we installed the wire-saving control system.

2.2 Interface Arm

An overview of the interface arm is shown in Fig. 7. The arm joint, including the first, second, and third joints, is actuated by an AC motor. The wrist joint, including the

TABLE 4
Specifications of the Interface Arm

Degrees of freedom		6 [DOF]	
Weight		under 3 [kg]	
Maximum output force(*)		over 56 [N]	
Workspace		0.09 [m^3]	
Operating angle of joints	1st / 2nd /3rd	-110~110 / -125~0 / 0~145	[deg]
	4th / 5th / 6th	-90~90 / -45~45 / -60~60	[deg]

(*) Maximum output force is not continous torque.

TABLE 5
Specifications of the Interface Arm Motors

Joint	Part number	Nominal torque [mNm]	Nominal current [A]	Gear ratio(*)
1st / 2nd / 3rd	maxon EC-max 30 272768	30.4	1.4	1972 / 1972 / 1062
4th	maxon RE-max 17 215996	3.13	0.116	1275
5th / 6th	maxon RE-max 17 216013	3.62	0.219	2431.5 / 1621

**The gear consists of the motor's gearhead and the gear of the transmission mechanism.*

fourth, fifth, and sixth joints, is actuated by a DC motor. The interface arm, therefore, has six joints allowing six DOF. Tables 4 and 5 show the specifications of the interface arm and of the motors, respectively. We used a motor with a brake for joints 2 and 3 in order to hold the arm in position after the power is turned off. Since we consider the performance and size of the motor as the selection criteria, and we were only able to find a suitable AC motor, we chose an AC motor for joints 2 and 3, and we used the same AC motor for joint 1 to create uniformity with joints 2 and 3.

The main improvements of the interface arm of HIRO III over that of HIRO II$^+$ are the following: 1) compactness, 2) a change in the layout of the first joint, 3) a reduction of the static friction at the joints, and 4) light weight. Regarding item 1, the interface arm of HIRO II$^+$ was designed to be as similar as possible to the human arm, as shown in Fig. 8. This design resulted to a large workspace, but a smaller workspace is sufficient to perform many tasks on a desktop. Thus, we designed the arm length of HIRO III to be shorter than that of HIRO II$^+$. On the other hand, HIRO II$^+$ has a 2-DOF shoulder joint, which allowed for shoulder adduction/abduction (first joint) and shoulder flexion/extension (second joint). When an operator uses HIRO II$^+$ and pushes the interface, its elbow part collides with the base. Therefore, we changed the layout of the first joint from shoulder adduction/abduction to shoulder radial/lateral rotation, which corresponds to item 2. We also made an offset between the first and second joints, as shown in Fig. 7. This helps to compensate for the reduced workspace. We note that HIRO III has no shoulder adduction/abduction; these motions are covered by the fourth joint. Regarding item 3,

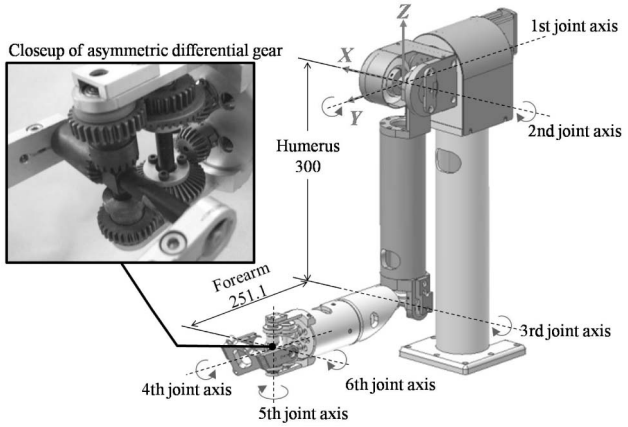

Fig. 8. Structure of the interface arm of HIRO II$^+$.

TABLE 6
Backlash and Friction Torque of the Interface Arm

	Joint	HIRO II$^+$	HIRO III
Backlash [deg]	1st / 2nd / 3rd	1.66 / 1.18 / 4.36	2.97 / 2.00 / 0.88
	4th / 5th / 6th	5.52 / 5.68 / 2.98	4.61 / 4.72 / 3.00
Static friction torque [Nm]	1st / 2nd / 3rd	3.07 / 1.91 / 1.36	2.04 / 1.76 / 0.87
	4th / 5th / 6th	0.18 / 0.42 / 0.17	0.04 / 0.19 / 0.02

we show the measurement results for the backlash and the static friction at the joints in Table 6. The method of measuring these values is the same as in the case of the haptic finger. Table 6 indicates that there was a large improvement in the static friction. The fifth and sixth joints stopped the use of the differential gear, and these joints work independently. Thus, we reduced the number of stages of the gear mechanism and saved weight in the joints, which helped to reduce the static friction. In particular, the transmission mechanism of the fifth joint was changed from the gear to the timing belt, and this change seems to have made a great improvement in the static friction. We realized a similar improvement by changing the transmission of the fourth joint to the timing belt as well. We noted that the backlash of the sixth joint was greater, because the transmission mechanism of the sixth joint was stopped, and the sixth joint axis was tied directly to the gearhead of the motor. We suspect that the backlash was due to the motor's gearhead. For the third joint, although there was no change in the number of stages of the gear, we believe that good performance was obtained as a result of the compactness and reduction of the weight of the interface arm. Like the sixth joint, the second joint axis was tied directly to the gearhead of the motor, and this influence seems to be reflected in the backlash. Since we changed the layout of the first joint, it is impossible to make a fair comparison of the first joint of HIRO III and the first joint of HIRO II$^+$.

As a result of addressing items 1 to 3, the weight of the interface arm was reduced to 3 kg, which is 43 percent of the weight of the interface arm of HIRO II$^+$, and item 4 was achieved. In the root of the interface arm, we created a box, and in it we installed the wire-saving control system for the interface arm.

3 Control System of HIRO III

To present the force at the five human fingertips, we installed 15 DC motors and five force sensors in the haptic hand of HIRO II$^+$. As a result, the communication cable between the PC and the haptic hand consists of 60 wires for the 15 encoders, 30 wires for the 15 motors, and 40 wires for the five force sensors. In addition, the interface arm of HIRO II$^+$ has six motors and six origin-seeking sensors, and the communication cables between the arm and the PC include 48 wires for the six encoders, 30 wires for the six motors, and 24 wires for the six origin-seeking sensors. Therefore, the total number of wires between the haptic interface and the control PC is 202. These wires greatly obstruct the smooth movement of the haptic interface. For example, the joint and the projection portion of the mechanism can become caught in the wires, and the external force exerted

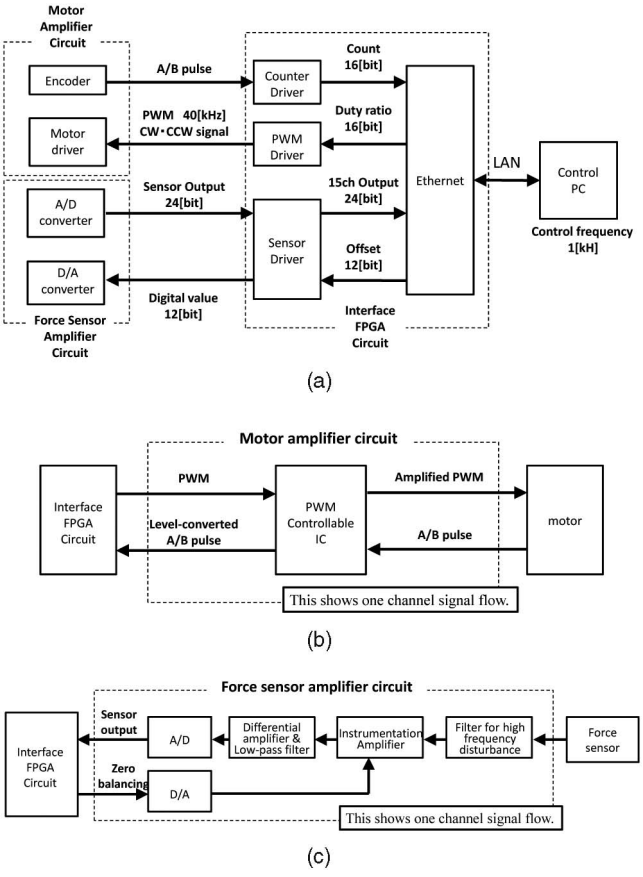

Fig. 9. Block diagram of the wire-saving control system for the haptic hand. (a) Overall signal flow. (b) Signal flow of the motor amplifier circuit. (c) Signal flow of the force sensor amplifier circuit.

by the wires affects the control of the haptic interface. Furthermore, the amplifiers of the force sensors and motors are stored under the haptic interface. Although the force sensor amplifiers and motor amplifiers are not large, many amplifiers are needed, and their combined size is large. Thus, to solve these problems, we have developed compact wire-saving control systems for the haptic hand and for the interface arm.

3.1 Control System for the Haptic Hand

The wire-saving control system for the haptic hand consists of the interface FPGA circuit, the force sensor amplifier circuit, and the motor amplifier circuit. Fig. 9 shows a block diagram of the communication among these circuits. In the FPGA, the VHDL language was used to create a counter driver to count the up/down pulses from the motor amplifier circuit, a PWM driver to provide the PWM outputs of 15 motors, and a sensor driver to read the digital values of the five force sensors and to provide the zero adjustment value of the five force sensors. The FPGA sends the sensors' signals to the control PC each time the PC sends the commands. When the PC sends the zero-adjustment signals of the force sensors, the FPGA sends digital signals corresponding to the zero-adjustment signals to the D/A converter in the force sensor amplifier circuit. In addition, the FPGA sends a PWM signal to the motor amplifier circuit when it receives the duty ratio signal from the control PC.

Fig. 10. Three-axis force sensor.

The main functions of the motor amplifier circuit are amplifying the 15-ch PWM signals from the FPGA circuit and converting the level of the 15-ch encoder signals. The signal flow of the motor amplifier circuit is shown in Fig. 9b. Fig. 9c shows the signal flow of the force sensor amplifier circuit. In the circuit, we installed a differential amplifier and a low-pass filter in the amplifier output of the sensor amplifier circuit, and we installed a 24-bit high-resolution A/D converter in the sensor amplifier circuit. With these measures, we believe we have achieved a high-precision force measurement. Furthermore, we installed a 12-bit D/A converter in the circuit because of the zero adjustment of the force sensors.

Fig. 10 shows the 3-axis force sensor, which was developed previously [30]. The sensor measures the 3-axis forces, F_x, F_y, and F_z, at the haptic fingertip. The force sensor is installed in the second link of each haptic finger and is connected to the sensor amplifier circuit. The force sensor must be small enough to install at the haptic fingertip. We set the following goals for the force sensor: 1) a low load can be measured, 2) its outside diameter is 14 mm, and 3) the interference between axis forces in the sensor element is minimal. By using the strain gauge in the pressure port of the sensor element, the force sensor measures the force from the deformation of the metal beam. The reasons for using the strain gauge are: 1) the sensor has better linearity, 2) the effect of the temperature change is small, and 3) the force sensor is suitable for the measurement of dynamic phenomena because the amount of displacement is extremely small. Fig. 11 shows the sensor structure of the 3-axis force sensor. For the acting axis force, the strain gauges are installed at the surface of the spot,

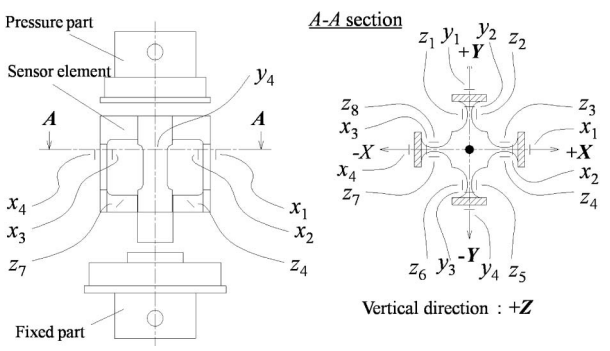

Fig. 11. Force sensor structure.

TABLE 7
Specifications of the Force Sensor

Rated capacity	5	[N]
Rated output (X-, Y- , Z-direction)	±0.3, ±0.3, ±0.1	[mV/V]
Safe overload	400	[%]
Nonlinearity, hysteresis	≤|1.0|	[%RO]
Repeatability	≤ 1.0	[%RO]
Size / Weight	Φ14×H27 [mm] / 12.8 [g]	

where the stress of the sensor element reaches a maximum, and the force is detected as a change in electrical resistance. The total number of strain gauges is 16: x_1-x_4, y_1-y_4, and z_1-z_8. For the forces in the X- and Y-directions, bending strains of x_1-x_4 and y_1-y_4, respectively, are detected. Further, shear strains of z_1-z_8 are detected for the force in the Z-direction. The specifications of the 3-axis force sensor are shown in Table 7.

The wire-saving control system for the haptic hand is installed in the space inside the handbase, as shown in Fig. 12. The force sensor, encoder, and motor signals are input into the control system and communicate with the control PC by an Ethernet connection. This allows us to reduce the number of wires between the haptic hand and the control PC from 115 to 10, including eight wires for the Ethernet and two wires for the power supply. The communication is fulfilled by UDP/IP and is a command-and-response type of communication. Since the retransmission processing is built into the control PC, the communication is reliable. We carried out several experiments, as described in Section 4. In these experiments, communication (sending and receiving) including latency was accomplished in 0.3 ms, and we were able to control HIRO III at a sufficient control rate (1 kHz). Table 8 shows the specifications of the wire-saving control system for the haptic hand.

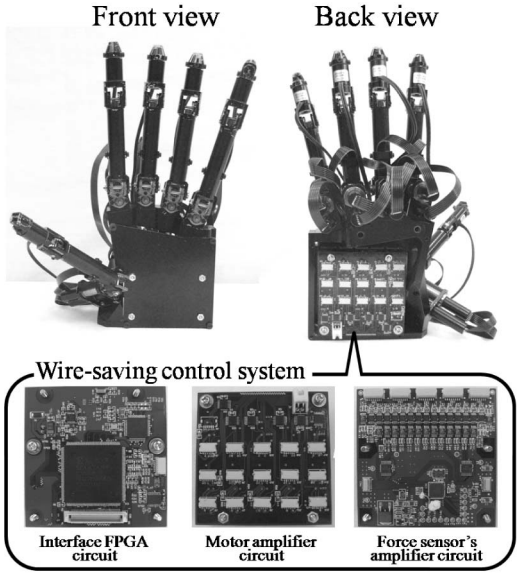

Fig. 12. Haptic hand in which the wire-saving control system is installed inside the handbase.

TABLE 8
Specifications: Wire-Saving Control System for the Haptic Hand

- Interface FPGA Circuit

Size	W70×D70×H1.6 [mm]
FPGA	Type: Xilinx Corp., Spartan3E(XCS500E)
	Clock frequency: 100 [MHz]
Ethernet	Communication: 100Base-TX, protocol: UDP

- Motor amplifier circuit

Size / Channel number	W70×D70×H4 [mm] / 15
Motor input signal form	PWM

- Force sensor amplifier circuit

Size / Channel number		W70×D70×H5 [mm] / 15
Amp. output	Differential amp.	Scale factor 2.5
	Low-pass filter	Cut-off freq. Fc = 100 [Hz]
ADC	Type / Resolution	ADS1258(Texas Instruments Inc.) / 24 [bit]
DAC	Type / Resolution	AD5328 (Analog Devices Inc.) / 12 [bit]

3.2 Control System for the Interface Arm

The wire-saving control system for the interface arm consists of the interface FPGA circuit and the motor amplifier circuit. Fig. 13 shows a block diagram of the communication between these circuits. The main differences from the hand control system are the following: 1) there is no force sensor amplifier circuit, and 2) a DIO driver was prepared in FPGA for the brakes of the motors and the origin-seeking sensors. The functions of PWM output, up/down count, and communication are the same as in the hand control system. Regarding the reset functions, in the interface arm, the second and third motors have brake systems that are connected to the motor amplifier circuit. The FPGA sends the on-off signal based on commands from the control PC,

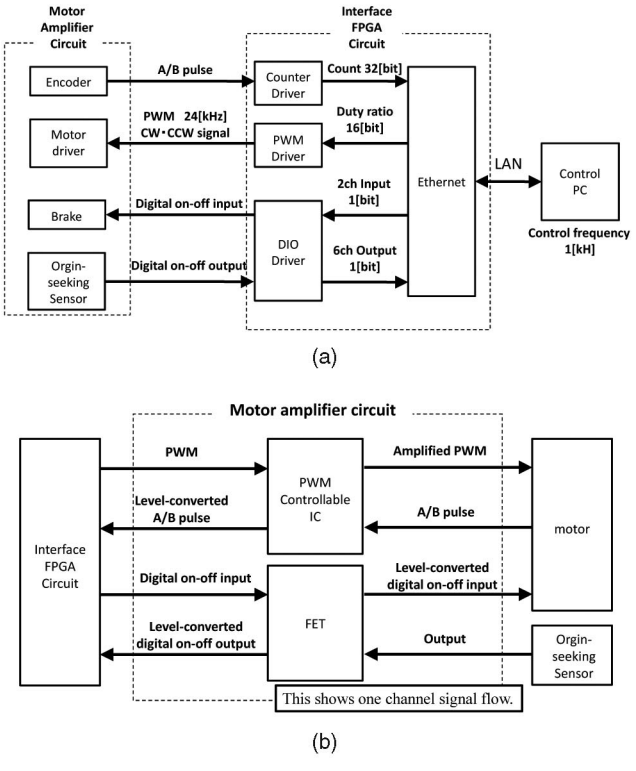

Fig. 13. Block diagram of the wire-saving control system for the Interface arm. (a) Overall signal flow. (b) Signal flow of the motor amplifier circuit.

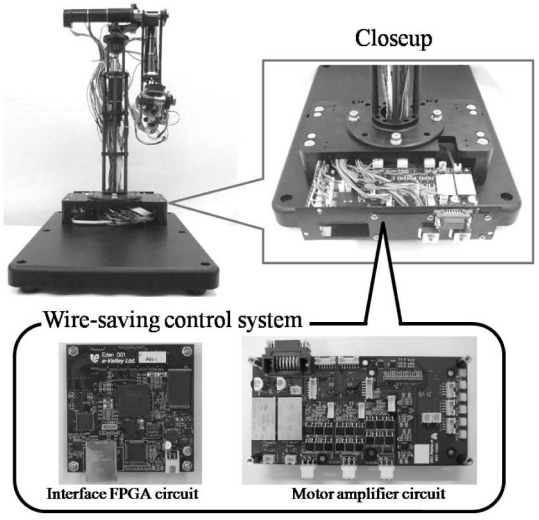

Fig. 14. Interface arm in which the wire-saving control system is installed inside the root.

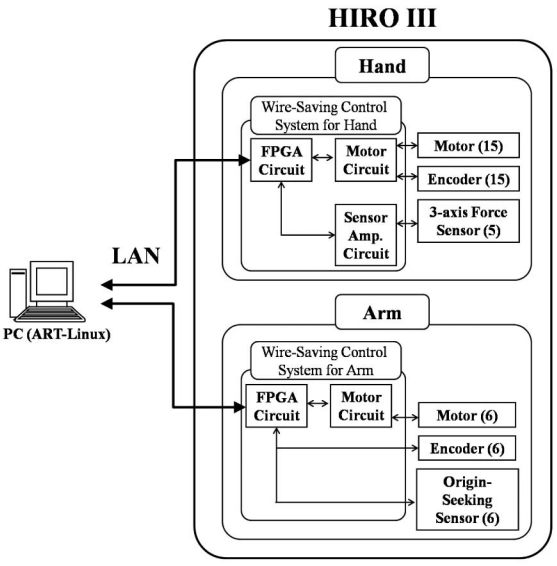

Fig. 15. Control system of HIRO III.

and the voltage conversion of the on-off signal is carried out in an FET (Field Effect Transistor) on the motor amplifier circuit. This on-off signal controls the brake. We used a photointerrupter as an origin-seeking sensor. The output of this sensor is input into the FET, and the on-off signal is created and input into the FPGA circuit. The FPGA sends this on-off signal to the control PC each time the PC sends the commands.

The wire-saving control system for the arm is installed in the space inside the box at the root of the interface arm, as shown in Fig. 14, and this system allows us to reduce the number of wires between the interface arm and the control PC from 90 to 10 (eight wires for the Ethernet and two wires for the power supply). Table 9 shows the specifications of the wire-saving control system for the interface arm.

By developing this compact wire-saving control system, we were able to reduce the number of wires between HIRO III and the control PC from 212 to 20, to increase the unit's compactness, and to improve the transportability of the total interface. Fig. 15 shows the control system of HIRO III.

4 Experiment

To evaluate HIRO III, we carried out several experiments. As the control law, we used the manipulability-optimized control [18]. This is a mixed control method consisting of a finger-force control and an arm position control intended to maximize the control performance index (3). The force control of the haptic finger is given by

$$\boldsymbol{\tau_F}(t) = \boldsymbol{K}_1 \boldsymbol{J}_{\boldsymbol{F}}^T \boldsymbol{F_e}(t) + \boldsymbol{K}_2 \boldsymbol{J}_{\boldsymbol{F}}^T \int_0^t \boldsymbol{F}_{\mathrm{e}}(s)\mathrm{d}s + \boldsymbol{J}_{\boldsymbol{F}}^T \boldsymbol{F_d} - \boldsymbol{K}_3 \dot{\boldsymbol{q}}_{\boldsymbol{f}}(t), \tag{1}$$

where $\boldsymbol{\tau}_F = [\boldsymbol{\tau}_1^T, \ldots, \boldsymbol{\tau}_5^T]^T \in \mathrm{R}^{15}$ is a joint torque vector of the haptic finger, J_F is a Jacobian, $\boldsymbol{F} = [\boldsymbol{F}_1^T, \ldots, \boldsymbol{F}_5^T]^T \in \mathrm{R}^{15}$ is a force vector whose sub vector is the force vector at the fingertip, $\boldsymbol{F_d} = [\boldsymbol{F}_{\boldsymbol{d}1}^T, \ldots, \boldsymbol{F}_{\boldsymbol{d}5}^T]^T \in \mathrm{R}^{15}$ is the desired force, $\boldsymbol{F_e} = \boldsymbol{F}_{\mathrm{d}} - \boldsymbol{F}$, and $\boldsymbol{q_f} = [\boldsymbol{q}_1^T, \ldots, \boldsymbol{q}_5^T]^T \in \mathrm{R}^{15}$ is a joint angle vector of the haptic finger. Furthermore, $\boldsymbol{K}_i$ is the positive feedback gain matrix. Here, the fourth term is the velocity feedback to employ the active damping. On the other hand, the control of the interface arm is given by the following PD (proportional and derivative) control with gravitational and external force compensators

$$\begin{aligned}\boldsymbol{\tau_A}(t) = {} & \boldsymbol{K}_{A1}(\boldsymbol{q}_{Ad} - \boldsymbol{q_A}) + \boldsymbol{K}_{A2}(\dot{\boldsymbol{q}}_{Ad} - \dot{\boldsymbol{q}}_{\boldsymbol{A}}) \\ & + \boldsymbol{g_A}(\boldsymbol{q_A}) + \boldsymbol{J}_A^T \begin{pmatrix} \sum_{i=1}^5 \boldsymbol{F_{di}} \\ \sum_{i=1}^5 (\boldsymbol{p_i} - \boldsymbol{p_{hb}}) \times \boldsymbol{F_{di}} \end{pmatrix},\end{aligned} \tag{2}$$

where $\boldsymbol{q_A} \in \mathrm{R}^6$ is the arm joint angle vector, $\boldsymbol{q_{Ad}} \in \mathrm{R}^6$ is the desired arm joint angle vector, which is to be determined, $\boldsymbol{\tau_A} \in \mathrm{R}^6$ is the interface arm joint torque, $\boldsymbol{K}_{Ai}$ is the positive feedback gain matrix, $\boldsymbol{g_A}(\boldsymbol{q_A})$ is the gravitational compensator term, $\boldsymbol{J}_A$ is a Jacobian, $\boldsymbol{p}_i \in \mathrm{R}^3$ is the ith fingertip position vector, and $\boldsymbol{p}_{hb} \in \mathrm{R}^3$ is the tip of the interface arm. Here, note that the desired arm joint angle vector $\boldsymbol{q_{Ad}}$ is defined to maximize the following control index (3) under a constraint condition in which the five haptic fingertip positions are fixed to the operator fingertip positions

TABLE 9
Specifications: Wire-Saving Control System for the Interface Arm

- Interface FPGA Circuit

Size	W70×D70×H15 [mm]
FPGA	Type: Xilinx Corp., Spartan3E (XCS1200E)
	Clock frequency: 100 [MHz]
Ethernet	Communication: 100 Base-TX, protocol: UDP

- Motor Amplifier Circuit

Size / Channel number	W170×D85×H17 [mm] / 6
Motor input signal form	PWM

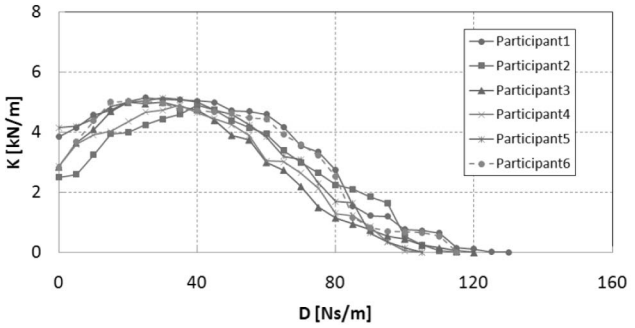

Fig. 16. Displayable region of the K-D plane.

$$\begin{aligned}
&\mathrm{CPI} = \sum_{i=1}^{5} (\alpha_i W_i + \beta_i P_i) + Q_A, \\
&W_i = \left(\det\left(\boldsymbol{J}_{Fi}^T \boldsymbol{J}_{Fi}\right)\right)^{\frac{1}{2}}, Q_A = -\frac{1}{2}(\boldsymbol{q}_{Ad} - \boldsymbol{q}_A)^T \Gamma (\boldsymbol{q}_{Ad} - \boldsymbol{q}_A), \\
&P_i = -\sum_{j=1}^{3} \gamma_j [\exp\{-\mu(q_{ij} - a_{ij})\} + \exp\{\mu(q_{ij} - b_{ij})\}],
\end{aligned} \tag{3}$$

where α_i and β_i are weighting coefficients, W_i is a manipulability measure of the ith finger, P_i is a penalty function to keep the finger joint angles within the movement range, γ_i is the weighting coefficient, μ is the parameter to adjust an exponential function, a_{ij} and b_{ij} are the lower and upper limits of the jth joint angle of the ith finger, Q_A is the penalty function to prevent a large change of the arm angle, and $\boldsymbol{\Gamma} > 0$ is a weighting matrix. Here, in the control, a finger/arm that reaches the limit of the movable range is switched to a position control to keep the joint angle in the movable range, and the rest joints of the fingers/arm are controlled by (1)/(2). After returning to within the movable range, the control is switched back again to (1)/(2). Details of the control law have been shown in [18].

In the above control, the feedback gain is constant. When a user manipulates the haptic interface in free space, the user feels the inertia and friction of the interface, and therefore, a high-gain feedback is desired. On the other hand, when a user uses the haptic interface in the constraint space, namely when the user contacts a virtual object, the high-gain feedback creates a vibrating response, and a low-gain feedback is desired. Therefore, in our experiments, we improved the force control of the haptic fingers include with nonconstant gain. The controller uses a high gain when the desired force is zero and a low gain when the desired force is not zero. For the experiment, the control PC used a real-time OS (ART-Linux) to guarantee a 1 ms sampling time.

4.1 Experiment 1

In the control of HIRO III, the force applied to the user's fingertips is provided by the force control of the haptic fingers. Therefore, to assess the basic force exertion performance, we considered the force exertion performance of HIRO III without using the interface arm in Experiment 1. First, we considered the displayable stiffness of HIRO III. To assess it, we carried out a contact experiment involving a virtual wall [32]. In this experiment, a user connected his/her index finger to the haptic index finger of HIRO III. We made a virtual wall by using a spring-damper model, and the desired force at the haptic finger was set to $\boldsymbol{F}_2^d = \boldsymbol{K}x_2 + \boldsymbol{D}\dot{\boldsymbol{x}}_2$, where $\boldsymbol{x}_2$ is the penetration depth of the second haptic finger into the virtual wall, and $\boldsymbol{K}$ and $\boldsymbol{D}$ are the stiffness and the damping coefficient of the virtual wall, respectively. Within view of the user, the virtual wall was set to a location about 2 mm away in the direction of the HIRO III (the Y-axis direction in Fig. 4). Six people, in their twenties, participated in the experiment. The experimental procedure was as follows: 1) a damping coefficient $\boldsymbol{D}$ was set, 2) the participant connected his/her index finger to HIRO III, and 3) the participant enlarged the stiffness coefficient $\boldsymbol{K}$ from 0 N/m at intervals of 50 N/m and the participant touched the virtual wall and moved his/her fingertips on the surface of the virtual wall in every case. If the participant felt the vibration, the stiffness coefficient $\boldsymbol{K}$ before one-step was the maximum displayable stiffness coefficient at the damping coefficient, which was set in Step 1). Then the participant returned to Step 1) and set the damping coefficient $\boldsymbol{D}$ to the next value. Six participants' displayable stiffnesses are shown in Fig. 16. In the figure, the region formed by the $\boldsymbol{D}$-axis, the $\boldsymbol{K}$-axis, and each participant's curve is the region, where the corresponding participant could feel the smooth surface of the virtual wall without any vibrations. We observed no large differences among the different subjects' curves, and the maximum displayable stiffness was about 5 kN/m.

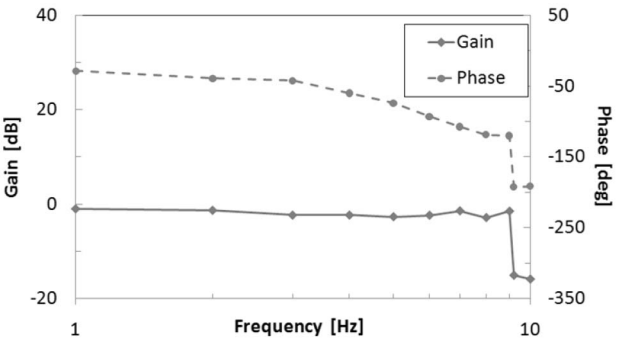

Fig. 17. Frequency response of force control: Y-axis.

In association with the above stiffness response, we also considered the frequency response of the force control. Fig. 17 shows the Y-axis frequency response of the haptic index finger. As the input of the force control, we selected the following sinusoidal function: $F_{d2} = [0, \sin(\omega t), 0]^T$, where $\omega = 2\pi f$ is the angular frequency and f is the frequency. As the output, we selected the Y-axis force of the haptic index fingertip. In the measurement, the operator connected his index finger to the haptic index finger, and the subject's finger was fixed to a bar, so that it could not move during the measurement. We considered frequencies f Hz from 0 to 10, and we measured the force response at each f three times. The mean value at each f is shown in Fig. 17. This figure shows only the Y-axis frequency response, but we also measured the X- and Z-axis responses, which were almost the same as the Y-axis result. The bandwidth of the force control was about 8 Hz, and we found that HIRO III could track high-speed motions of the operator such as tapping.

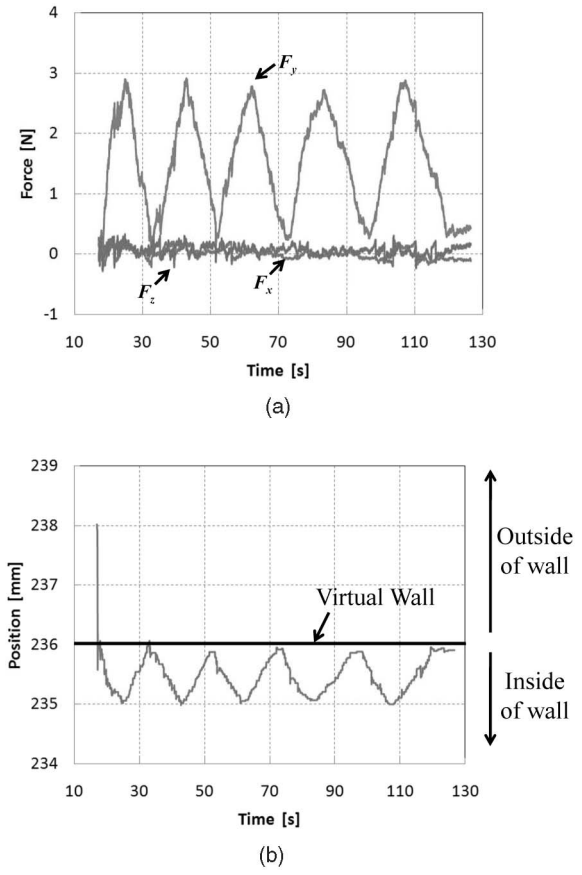

Fig. 18. Force and position responses of the haptic index finger. (a) Force responses. (b) Position response.

Finally, we considered the force responses of the haptic finger using the same experimental environment as in the contact experiment described above. In this case, the participant connected his index finger to the haptic index finger and pushed the virtual wall several times. The stiffness coefficient $\boldsymbol{K}$ and the damping coefficient $\boldsymbol{D}$ of the virtual wall were set at $\boldsymbol{K} = 3$ kN/m and $\boldsymbol{D} = 50$ Ns/m. Fig. 18a shows the three-axis force responses of the haptic index finger. The virtual wall was set at a location about 2 mm away in the Y-axis direction, and thus the desired force was set at $\boldsymbol{F}_{d2} = [0, Kx_2 + D\dot{x}_2, 0]^T$. The average force errors of the X-, Y-, and Z-axes were 0.07, 0.16, and 0.08 N, respectively, and the total average force error was 0.10 N. Since human fingers can only sense force variations as small as 0.5 N [33], these force errors are sufficiently small.

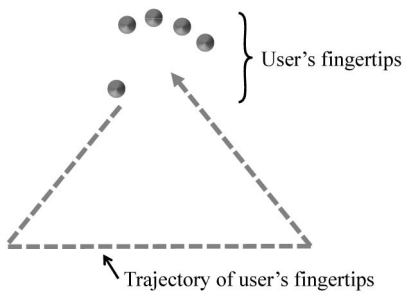

Fig. 19. Trajectory of the user's fingertips in experiment 2.

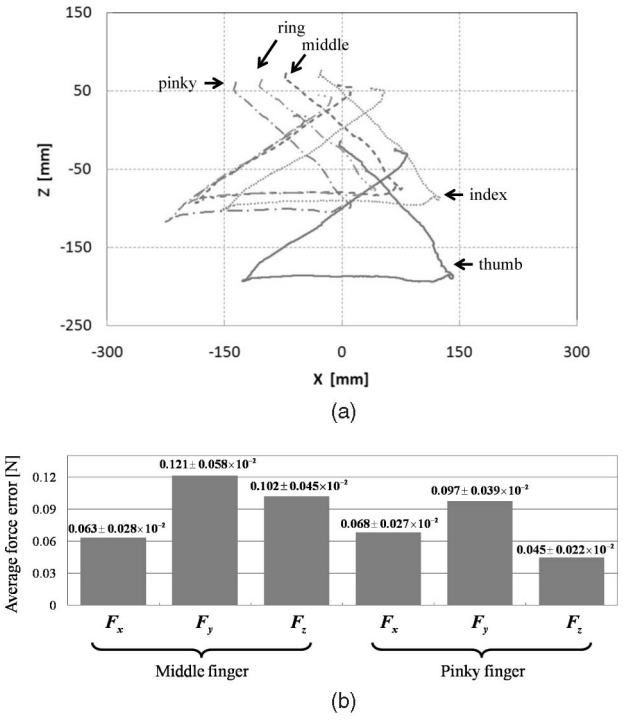

Fig. 20. Responses in free space. (a) Position responses. (b) Average force errors of the middle and pinky fingers.

Fig. 18b shows the Y-axis fingertip position of the haptic index finger. The figure also shows the position of the virtual wall. From this figure, we can confirm that the participant moved his finger to the virtual wall and then pushed the virtual wall. Note that the participant kept touching the virtual wall until the moment the measurement was finished. In addition, we also considered the force response of the haptic finger in free space. The desired force of the index finger was set at $\boldsymbol{F}_{d2} = [0, 0, 0]^T$. The operator connected his index finger to the haptic index finger and then shuttled his finger along the Y-axis. The amplitude of the shuttle was 2 cm. The average force errors of the X-, Y-, and Z-axes were 0.04, 0.06, and 0.05 N, respectively, and the total average value was 0.05 N. Compared with the virtual wall experiment, in which the desired force was not 0, the force errors of all axes were small.

4.2 Experiment 2

Next, we considered the motion performance of HIRO III using the haptic hand and the interface arm. The operator's five fingers were connected to HIRO III, and the operator manipulated HIRO III in free space so as to draw a triangle in VR space, as shown in Fig. 19. Here, note that the operator was not instructed to track a virtual triangular target, but was allowed to execute any size of triangular trajectory that he or she desired.

Fig. 20 shows the responses of HIRO III in free space. Fig. 20a shows the responses of the five fingertip positions of HIRO III, while Fig. 20b shows the average force errors of the middle and pinky fingertips of HIRO III. (For the X- and Z-axes in Fig. 20a, see the axes in Fig. 21.) Since we were considering the manipulation of HIRO III in free space, the desired forces at the five fingertips were set to 0. However,

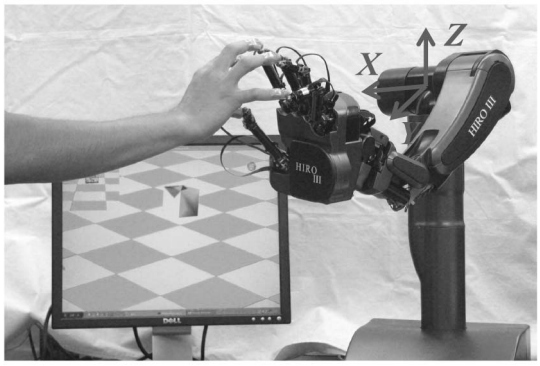

Fig. 21. Experimental environment.

the responses of the fingertip forces show a slight force error. The average force errors of each finger were 0.093 N for the thumb, 0.091 N for the index finger, 0.095 N for the middle finger, 0.072 N for the ring finger, and 0.070 N for the pinky, and the total average force error was 0.084 N (we showed the average force errors of the fingers with the largest and smallest force errors in Fig. 20b). The numerical values in Fig. 20b represent the average force error $\pm$ the standard error of the mean. The total average force error of HIRO II^{+} in free space was 0.173 N. Therefore, the responses of HIRO III in free space were apparently improved, and the average force error was reduced to 48.5 percent. The interface arm has a large load (the arm's own weight and the weight of the haptic hand), and thus, the result of Experiment 2 was slightly less favorable in terms of force presentation than the result of Experiment 1, which involved only the haptic finger. This is equivalent to saying that the inertia of the arm reduces the transparency of the system. In this paper, we did not consider the compensation for the arm's inertia, but it is a very important topic. To improve the transparency, we will need to design a dynamic control law that compensates for the inertia as done the control law in [34] as the next problem to be tackled. Note that, however the users remarked that they could manipulate HIRO III smoothly.

In this experiment, the average fingertip velocity was 32.9 mm/s, which is relatively slow. As a high-speed motion case, we measured the force error when the operator manipulated HIRO III at high speed (72.9 mm/s). The average force error of the five fingertips was 0.265 N. Although this value is three times higher than the force error during the slow motion, it is still a small value. The same observation could be made about Experiment 3. Note that, because of safety constraints, our current research did not target high-speed motion. In the future, the performance (force error) during high-speed motion must be improved so that it is similar to that achieved in slow motion. On the other hand, the connection between the operator and HIRO III is accomplished by permanent magnets. The breaks in these connections depend not on the manipulation speed of HIRO III but on the force, with which the operator pulls his/her fingers from HIRO III. Currently, the permanent magnet connection breaks if the operator pulls his/her finger with a force of about 4.3 N.

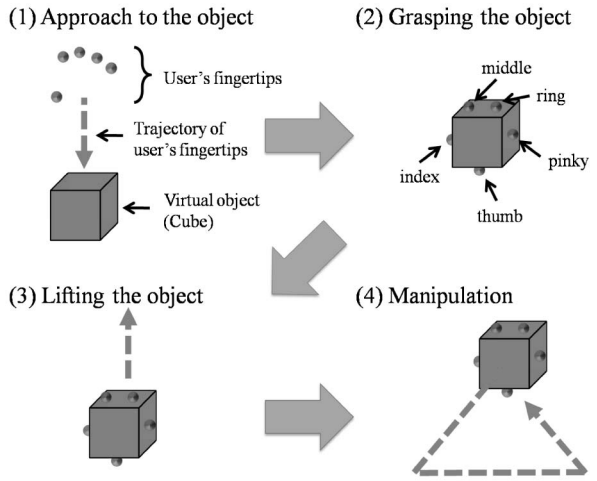

Fig. 22. Experimental procedure.

4.3 Experiment 3

Finally, we considered the manipulation ability of HIRO III in a constraint space using the haptic hand and the interface arm. In the experiment, the operator's five fingers were connected to the haptic interface, and the operator moved his five fingertips as shown in Fig. 22. The operating procedure was as follows: 1) the operator approached the virtual cubic object, 2) the operator grasped the object, 3) the operator lifted the object, and 4) the operator drew a triangle while grasping the cube in the VR space.

The force displayed at the ith human fingertip (the desired force) is $\boldsymbol{f}_i = \boldsymbol{f}_i^c + \boldsymbol{f}_i^f$, where $\boldsymbol{f}_i^c$ and $\boldsymbol{f}_i^f$ are the constraint and the friction force of the ith fingertip, respectively. In the experiment, when the finger contacts the virtual object, we set $\boldsymbol{f}_i^c$ and $\boldsymbol{f}_i^f$ at each finger as the following: $\boldsymbol{f}_i^c = K\boldsymbol{a}_i^n + D\boldsymbol{v}_i^n$,

$$\boldsymbol{f}_i^f = \begin{cases} \left(\eta_i \|\boldsymbol{f}_i^c\| + d\boldsymbol{t}_i^T \boldsymbol{v}_i\right)\boldsymbol{t}_i \\ \quad \text{(in the case of the static frictional force)}, \\ \left(\lambda_i \|\boldsymbol{f}_i^c\| + \gamma_i \boldsymbol{t}_i^T \boldsymbol{v}_i\right)\boldsymbol{t}_i \\ \quad \text{(in the case of the dynamic frictional force)}, \end{cases}$$

where the penetration depth vector of the ith finger into the object is decomposed to a normal directional vector a_i^n and a frictional directional vector a_i^t, v_i^n is the relative speed between the fingertip velocity and object velocity, K is the stiffness of the object, and D is the damping coefficient of the object. Furthermore, η_i is the coefficient of static friction given by $\eta_i = \|\boldsymbol{a}_i^t\|/\|\boldsymbol{a}_i^n\|, d$ is the damping coefficient, λ_i is the coefficient of the dynamic frictional force, γ_i is the damping coefficient at the dynamic friction state, and $\boldsymbol{t}_i$ is the unit vector of the frictional force direction. In the experiment, we set $K = 300, D = 1.0 \times 10^{-3}, d = 1.5, \lambda_i = 0.5$, and $\gamma_i = 0$. (For the technical details, please see [35].)

Fig. 23 shows the responses in the constraint space. Fig. 23a shows the response of the thumb fingertip of HIRO III. From Fig. 23a, it is obvious that the operating procedure 1-4 were followed. Figs. 23b and 23c show the responses of the thumb and the pinky fingertip force of HIRO III, respectively. The average force errors of each finger were the following: 0.237 N for the thumb, 0.138 N for the index

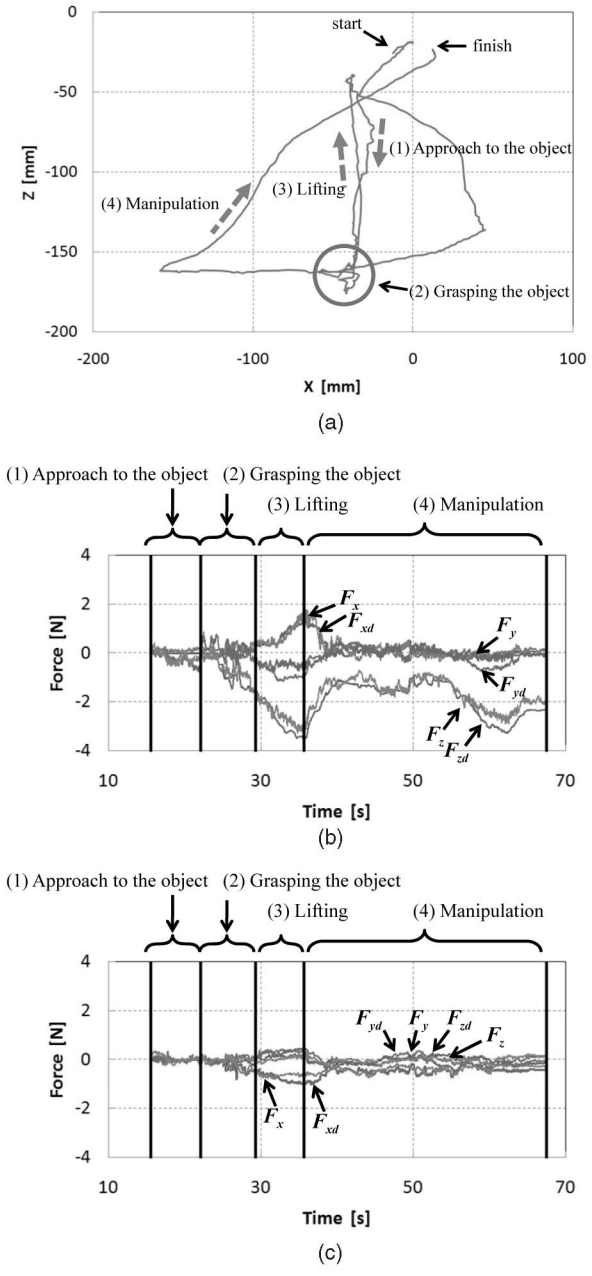

Fig. 23. Responses in constraint space. (a) Position responses: Thumb. (b) Force response: Thumb. (c) Force response: Pinky finger.

finger, 0.132 N for the middle finger, 0.199 N for the ring finger, and 0.129 N for the pinky. Total average force error was 0.167 N. Since the responses of the thumb and pinky had the largest and smallest force errors, respectively, we showed these fingertips' responses in Fig. 23b and 23c. The force response of the axis with a large desired value has a larger force error than the force response of the axis with a small desired value. However, the force error is about 0.2 N, and we feel that HIRO III had good force tracking performance. On the other hand, the performance of HIRO III with the haptic hand and the interface arm is inferior to the performance of HIRO III using only the haptic hand (the result of Experiment 1). This result is approximately the same in the case of manipulation in free space.

5 Conclusion

We have described a newly developed five-fingered haptic interface robot, known as HIRO III. A new design mechanism for a haptic hand and interface arm was introduced, and the following functionality requirements of the haptic interface were achieved: a reduction of the static friction at the joint, a change in the connect position between the human and haptic fingertips to enable better grasping of a virtual object, greater compactness in size, and lighter weight. Furthermore, we have developed a compact wire-saving control system for the haptic hand and the interface arm. These systems are installed in the space inside the haptic interface. The force sensor, encoder, motor, brake for the motor, and zero-seeking sensor signals are input into the system and communicate to the main control PC on an LAN. This reduces the number of wires in the control system, increases compactness, and improves the transportability of the total interface. Finally, we carried out several experiments, the results of which showed the high-precision force presentation and the high potential of HIRO III.

Although the reduction of static friction at the joints was accomplished by changing the transmission mechanism by incorporating asymmetric differential gears, reducing the weight of the interface, and so on, we were not able to reduce the backlash at the joints. At the present stage, we consider that the motor's gearhead has the largest influence, and changing the gearhead is one of our future tasks. In addition, the inertia of the arm influences the performance of the force control of the haptic interface in the experiments. In this paper, we did not consider compensating for the inertia of the arm, but we will need to devise a dynamic control law that compensates for the interface arm's inertia as the next problem to be tackled. Furthermore, as an application of HIRO III, we have researched and developed bimanual haptic interface that can present three-directional force at the ten human fingertips of both hands.

Acknowledgments

This paper was supported by the Ministry of Internal Affairs and Communications Strategic Information and Communications R&D Promotion Programme (SCOPE). The authors thank Prof. S. Nakagawa for cooperating with the cover design of HIRO III.

References

[1] N. Magnenat-Thalmann and U. Bonanni, "Haptics in Virtual Reality and Multimedia," *IEEE Multimedia*, vol. 13, no. 3, pp. 6-11, July-Sept. 2006.

[2] F. Barbagli, K. Salisbury, and R. Devengenzo, "Toward Virtual Manipulation: From One Point of Contact to Four," *Sensor Rev.*, vol. 24, no. 1, pp. 51-59, 2004.

[3] Z. Najdovski and S. Nahavandi, "Extending Haptic Device Capability for 3D Virtual Grasping," *Haptics: Perception, Devices and Scenarios (Proc. Sixth Int'l Conf. EuroHaptics 2008)*, M. Ferre ed., pp. 494-503, Springer, 2008.

[4] G. Jansson, M. Bergamasco, and A. Frisoli, "A New Option for the Visually Impaired to Experience 3D Art at Museums: Manual Exploration of Virtual Copies," *Visual Impairment Research*, vol. 5, pp. 1-12, 2003.

[5] S. McKnight, N. Melder, A. Barrow, W. Harwin, and J. Wann, "Psychophysical Size Discrimination Using Multi-Fingered Haptic Interfaces," *Proc. EuroHaptics 2004*, pp. 274-281, 2004.

[6] B. Van DerHorst and A. Kappers, "Curvature Discrimination in Various Finger Conditions," *Experimental Brain Research,* vol. 177, pp. 304-311, 2007.

[7] A. Frisoli, F. Simoncini, M. Bergamasco, and F. Salsedo, "Kinematic Design of a Two Contact Points Haptic Interface for the Thumb and Index Fingers of the Hand," *ASME J. Mechanical Design* , vol. 129, pp. 520-529, 2007.

[8] M. Srinivasan and C. Basdogan, "Haptics in Virtual Environments: Taxonomy, Research Status, and Challenges," *Computer and Graphics,* vol. 21, no. 4, pp. 393-404, 1997.

[9] S. Walairacht, M. Ishii, Y. Koike, and M. Sato, "Two-Handed Multi-Fingers String-Based Haptic Interface Device," *IEICE Trans. Information and Systems,* E84D, pp. 365-373, 2001.

[10] Y. Ueda and T. Maeno, "Development of a Mouse-Shaped Haptic Device with Multiple Finger Inputs," *Proc. IEEE/RSJ Int'l. Conf. Intelligent Robots Systems,* vol. 3, pp. 2886-2891, 2004.

[11] R. Leaschke, E. Kurihara, J. Dosher, and B. Hannaford, "High Fidelity Multi Finger Haptic Display," *Proc. World Haptics Conf. (WHC '05),* pp. 606-608, 2005.

[12] M. Monroy, M. Oyarzabal, M. Ferre, A. Camposv, and J. Barrio, "MasterFinger: Multi-Finger Haptic Interface for Collaborative Environments," *Haptics: Perception, Devices and Scenarios (Proc. Sixth Int'l Conf. EuroHaptics 2008),* M. Ferre ed., pp. 411-419, Springer, 2008.

[13] M. Kawai and T. Yoshikawa, "Stable Haptic Display of 1-DOF Grasping with Coupling Impedance for Internal and External Forces," *Proc. IEEE/RSJ Int'l. Conf. Intelligent Robots Systems,* pp. 1316-1321, 2000.

[14] S. Wall and W. Harwin, "Design of a Multiple Contact Point Haptic Interface," *Proc. EuroHaptics 2001,* pp. 146-148, 2001.

[15] A. Coutee, S. McDermott, and B. Bras, "A Haptic Assembly and Disassembly Simulation Environment and Associated Computational Load Optimization Techniques," *ASME J. Computing and Information Science Eng.,* vol. 1, pp. 113-122, 2001.

[16] CyberGlove Systems, CyberForce, http://www.cyberglovesystems.com/products/hardware/cyberforce.php. 2010.

[17] A. Frisoli, F. Rocchi, S. Marcheschi, A. Dettori, F. Salsedo, and M. Bergamasco, "A New Force-Feedback Arm Exoskeleton for Haptic Interaction in Virtual Environment," *Proc. World Haptics Conf. (WHC '05),* pp. 191-201, 2005.

[18] S. Tachi, N. Kawakami, H. Nii, K. Watanabe, and K. Minamizawa, "TELEsarPHONE: Mutual Telexistence Master-Slave Communication System Based on Retroreflective Projection Technology," *SICE J. Control, Measurement, and System Integration,* vol. 1, no. 5, pp. 335-344, Sept. 2008.

[19] Y. Adachi, T. Kumano, A. Ikemoto, A. Hattori, and N. Suzuki, "Development of a Haptic Device for Multi Fingers by Macro-Micro Structure," *J. Robotics Soc. Japan,* vol. 20, no. 7, pp. 725-733, 2002.

[20] H. Maekawa and J. Hollerbach, "Haptic Display for Object Grasping and Manipulating in Virtual Environment," *Proc. IEEE Int'l Conf. Robotics and Automation,* pp. 2566-2573, 1998.

[21] Y. Yokokohji, N. Muramori, Y. Sato, and T. Yoshikawa, "Designing an Encountered-Type Haptic Display for Multiple Fingertip Contacts Based on the Observation of Human Grasping Behaviors," *The Int'l J. Robotics Research,* vol. 24, pp. 717-729, 2005.

[22] H. Kawasaki and T. Hayashi, "Force Feedback Glove for Manipulation of Virtual Objects," *J. Robotics and Mechatronics,* vol. 5, no. 1, pp. 79-84, 1993.

[23] M. Bouzit, G. Burdea, G. Popescu, and R. Boian, "The Rutgers Masster II - New Design Force-Feed BackGlove," *IEEE/ASME Trans. Mechatronics,* vol. 7, no. 2, pp. 256-263, June 2002.

[24] CyberGlove Systems, CyberGrasp, http://www.cyberglovesystems.com/products/hardware/cybergrasp.php. 2010.

[25] T. Koyama, I. Yamano, K. Takemura, and T. Maeno, "Multi-Fingered Exoskelton Haptic Device Using Passive Force Feedback for Dexterous Teleoperation," *Proc. IEEE/RSJ Int'l Conf. Intelligent Robots Systems,* pp. 2905-2910, 2002.

[26] A. Saddik, "The Potential of Haptics Technologies," *IEEE Instrumentation and Measurement,* vol. 10, no. 1, pp. 10-17, Feb. 2007.

[27] H. Kawasaki, J. Takai, Y. Tanaka, C. Mrad, and T. Mouri, "Control of Multi-Fingered Haptic Interface Opposite to Human Hand," *Proc. IEEE/RSJ Int'l Conf. Intelligent Robots Systems,* pp. 2707-2712, 2003.

[28] H. Kawasaki and T. Mouri, "Design and Control of Five-Fingered Haptic Interface Opposite to Human Hand," *IEEE Trans. Robotics,* vol. 23, no. 5, pp. 909-918, Oct. 2007.

[29] R. Ellis, O. Ismaeil, and M. Lipsett, "Design and Evaluation of a High-Performance Haptic Interface," *Robotica,* vol. 12, pp. 321-327, 1996.

[30] T. Endo, Y. Kawachi, H. Kawasaki, and T. Mouri, "FPGA-Based Control for the Wire-Saving of Five-Fingered Haptic Interface," *Haptics: Perception, Devices and Scenarios (Proc. Sixth Int'l Conf. EuroHaptics 2008),* M. Ferre ed., pp. 536-542, Springer, 2008.

[31] T. Mouri, H. Kawasaki, K. Yoshikawa, J. Takai, and S. Ito, "Anthropomorphic Robot Hand: Gifu Hand III," *Proc. Int'l. Conf. Control, Automation and Systems (ICCAS '02),* pp. 1288-1293, 2002.

[32] J. Colgate and J. Brown, "Factors Affecting the Z-Width of a Haptic Display," *Proc. IEEE Int'l Conf. Robotics Automation,* pp. 3205-3210, 1994.

[33] K. Shimoga, "A survey of Perceptual Feedback Issues in Dexterous Telemanipulation: Part I. Finger Force Feedback," *Proc. IEEE Virtual Reality Ann. Int'l. Symp.,* pp. 263-270, 1993.

[34] T. Yoshikawa and A. Nagura, "A Touch/Force Display System for Haptic Interface," *Presence,* vol. 10, pp. 225-235, 2001.

[35] H. Kawasaki, Y. Ohtuka, M.O. Alhalabi, and T. Mouri, "Haptic Rendering and Perception of Frictional Moment," *Proc. EuroHaptics Conf.,* pp. 201-206, 2006.

Takahiro Endo received the DrEng degree from Tokyo Institute of Technology, Tokyo, Japan, in 2006. Since April 2006, he has been an assistant professor in the Faculty of Engineering, Gifu University, Gifu, Japan. His research interests include haptic interfaces, robotics, and control of infinite dimensional systems. He is a member of the IEEE.

Haruhisa Kawasaki received the MS and doctoral degrees from the Nagoya University, Japan, in 1974 and 1986, respectively. He is currently a professor in the Faculty of Engineering, Gifu University, Japan. From 1974 to 1990, he was a research engineer at NTT's laboratories. After that, he was a professor with the Kanazawa Institute of Technology from 1990 to 1994. From July 1998 to January 1999, he was a visiting professor at University of Surrey (United Kingdom). His research interests include areas of robot control, humanoid robot hand, haptic interface in virtual reality, and computer algebra of robotics. He has contributed himself to the community as a member of many organizations, such as the Institute of Electrical and Electronic Engineers (IEEE), the Japan Society of Mechanical Engineers (JSME), the Robotics Society of Japan (RSJ), the Society of Instrument and Control Engineers (SICE), and the Virtual Reality Society of Japan (VRSJ). He is a fellow of JSME and RSJ. He has received several awards, such as the Best Paper Award of the World Automation Congress 2004, the Prizes for Science and Technology of The Commendation for Science and Technology by the Minister of Education, Culture, Sports, Science and Technology of Japan 2006, and JSME Funai Award 2009. He was the National Organizing Committee chair of the 9th International IFAC Symposium on Robot Control (SYROCO 2009). He is a senior member of the IEEE and the IEEE Computer Society.

Tetsuya Mouri received the MS and PhD degrees in mechanical engineering from the Nagoya Institute of Technology, Nagoya, Japan, in 1997 and 2000, respectively. He is currently an associate professor with the Faculty of Engineering, Gifu University, Gifu, Japan. His research interests include the areas of humanoid robot hand, haptic interface in virtual reality, and identification of contact conditions. He is a member of the IEEE.

Yasuhiko Ishigure joined Marutomi Seiko Co., Ltd. in 1999, and has been active in R&D on the rehabilitation support systems, multifingered haptic interface, and pruning robot. He is a member of the Robotics Society of Japan (RSJ).

Hisayuki Shimomura received the BS degree in metal engineering from the Faculty of Engineering, Iwate University, Iwate, Japan, in 1965. From 1965 to 1972, he was with Nihon Kentetsu Inc., Japan, where he was involved in research and development of a washing machine. In 1972, he joined Iron Works Co., Ltd. Dainichi (Dainichi Co., Ltd), Japan, where he was the president during 1981-2009. He is currently the chairman of Dainichi Co., Ltd. Since 1996, he has been active in research and development of the robot hand, and has received several awards, such as the Technical Innovations Awards 2003 by the Robotics Society of Japan, and the Prizes for Science and Technology of The Commendation for Science and Technology by the Minister of Education, Culture, Sports, and Science and Technology of Japan, in 2006. Dainich Co., Ltd was selected as 300 Japan's Dynamic Monodzukuri, manufacturing, SMEs supporting the Japan of Tomorrow by Ministry of Economy, Trade and Industry, in 2007, and received the funding support of SMEs' product development and manufacturing by Ministry of Economy, Trade and Industry, in 2009.

Masato Matsumura received the BE degree in electrical and electronic engineering from the Faculty of Science and Technology, Meijo University, Nagoya, Japan, in 1983. He is currently the director of e-Valley Co.,Ltd. His research interests include haptic interfaces and robotics.

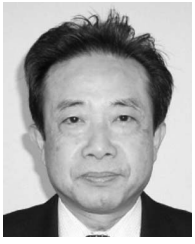

Kazumi Koketsu was with the tech wing of a major measuring instrument manufacturer. In 1991, he established Tec Gihan Corporation and is currently its president.